The EXAFS study of nanocrystalline zirconia

1994 J. Phys.: Condens. Matter 6 633

(http://iopscience.iop.org/0953-8984/6/3/005)

J. Phys.: Condens. Matter 6 (1994) 633–640. Printed in the UK

The EXAFS study of nanocrystalline zirconia

Wang Yuren†, Lu Kunquan‡, Wang Dazhi§, Wu Zhonghua‡ and Fang Zhengzhi†

† University of Science and Technology of Beijing, Beijing 100083, People's Republic of China

‡ Institute of Physics, Chinese Academy of Sciences, Beijing 100080, People's Republic of China

§ University of Science and Technology of China, Hefei 230026, People's Republic of China

Received 29 September 1993

Abstract. We performed temperature-dependent extended x-ray absorption fine structure (EXAFS) measurements on a series of nanocrystalline zirconia powders with different crystallite sizes. The results show that there is a tetragonal-to-cubic phase transition with reduction of crystallite size. The temperature dependence of the EXAFS Debye–Waller factor is also discussed.

1. Introduction

During the last decade, nanocrystalline materials (typically having crystallite size of just a few nanometres) have been of much interest because novel properties appear in these materials, such as the enhanced plasticity of a nanocrystalline ceramic material [1] and the high diffusivity of Ag in nanocrystalline Cu [2]. Hence, nanocrystalline materials will be applied widely in technology.

It is well known that the properties of a material are closely connected with its atomic structure, so structure determination is very important for good understanding of structure-dependent properties. Many techniques have been applied to probe the atomic structure of nanocrystalline materials, for instance, x-ray diffraction [3], high-resolution electronic microscopy [4, 5], positron lifetime spectroscopy [6] and Mossbauer spectroscopy [7], while extended x-ray absorption fine structure (EXAFS) spectroscopy is also a powerful tool for the identification of the atomic structure, particularly for the identification of the local structure around absorbing atoms. Many EXAFS studies have been made of the local atomic structure in nanocrystalline materials or small clusters [8–11]. Most of these studies focused on metal clusters. Few investigations were made of the nanocrystalline oxides. Nanophase oxides, such as TiO_2, Fe_2O_3 and ZrO_2, have high catalysis activity and other particular properties. EXAFS studies on these materials are important.

Yttria-stabilized zirconia is an important anion-conducting ceramic. Pure zirconia at room temperature (RT) is in monoclinic form. The monoclinic (m)-to-tetragonal (t) phase transition was found at about 1174 °C and another transition from the t to the cubic (c) phase took place at about 2300 °C. However, the t phase appears at RT when the crystallite size is of nanometre order [12, 13]. Furthermore, diffraction studies [14, 15] of the ultradispersed powder of zirconia also indicated that its structure could be described in the t crystal system, and the lattice parameters approached those in the CaF_2 c phase with further reduction of the particle size. The accuracy of the lattice parameters and the structural symmetry determined by the diffraction methods is limited by the broadening of peaks, when the particle size is

0953-8984/94/030633+08$07.50

of nanometre order. For zirconia, the diffraction pattern of the t phase is very similar to that of the c phase. This makes the identification of structural symmetry more difficult. However, the local structure in the t phase is different from that in the c phase. Using the EXAFS technique, the difference between the local atomic structures in the two phases can be detected and used to identify the phase of the sample.

In this paper, we report the results of EXAFS measurements for a series of ultrafine zirconia powders with different mean particle sizes. The possible t–c phase transition versus the particle size is deduced from the results and the temperature-dependent variations of Debye–Waller factors are also discussed.

2. Experiment

2.1. Sample preparation

Nanosized zirconia powders were prepared by the coprecipitation method. 7 mol% yttria-stabilized zirconia powder was prepared by the coprecipitation–spray-drying method from zirconium oxychloride and yttria (dissolved in HNO_3 before use). The precipitated cake was washed with distilled water to remove anions, and then with alcohol twice to replace water in the cake. The cake was then made into slurry, which was followed by spray-drying in a mini-spray-dryer (Brikmann/Buchi Model 190, Westbury, NY), and further calcinated at different temperatures to obtain different sizes of crystallite. By this method, three samples with different mean particle size were prepared.

Chemical analysis and x-ray fluorescence spectroscopy (SRFS, PW 1404) were adopted for the quantitative analysis of the main components. Atomic emission spectroscopy (ICP 3589) was employed for the qualitative analysis of the whole elements, while atomic absorption spectroscopy (ICP 5000) was used to analyse impurity quantitatively. The results are shown in table 1. The mean particle sizes of the three prepared samples were about 5 nm, 8 nm and 11 nm, as estimated by the x-ray diffraction method. For convenience, the three prepared samples are denoted as Zr1, Zr2 and Zr3 respectively.

Table 1. Content of components in the prepared nanosized zirconia powder.

	ZrO_2	Y_2O_3	HfO_2
Content (mol%)	91.68	7.27	1.05

The samples used in the EXAFS experiment were prepared in the following way. The nanometre-sized powders were sieved through 400 mesh screening and then smeared uniformly onto Scotch tape. Several layers were used to achieve the optimum thickness ($\mu d \leqslant 1.5$, $\Delta\mu x = 1.0$). The bulk samples of m zirconia (MZ) and yttria-stabilized c zirconia (YCZ, 10 mol% yttrium content) were prepared in the same way.

2.2. EXAFS experimental details

We measured the Zr K-edge absorption for all of the samples at three temperatures (i.e., 70 K, 140 K and 210 K). The XAFS spectra were measured on Beemline 4W1B at the radiation source of Beijing Synchrotron Radiation Laboratory. A transmission mode was used in the measurement with an Si(111) double-crystal monochromator. The electron energy in the storage ring was about 2.2 GeV with a current of about 20 mA. The photon

intensity at the sample is about 10^8 counts s^{-1}. Two ion chambers filled with a mixture of Ar and N_2 gas were used to detect both incident x-ray intensity I_0 and transmitted intensity I simultaneously. The Y K edge (17 038 eV) was used to calibrate the energy scale. The monochromator was detuned to eliminate the high-order harmonics. The energy resolution at 17 keV was estimated to be about 2 eV. For each sample several independent scans were performed to examine the repetition of experimental data and estimate error bars.

3. Data analysis and results

The x-ray absorption spectra were analysed using a standard procedure [16]. The EXAFS oscillations were isolated after the subtraction of the pre-edge contribution, background removal and normalization. Figure 1 shows the EXAFS spectra, $\chi(k)$, of nanocrystalline zirconia, YCZ and yttrium-stabilized t zirconia (YTZ). It can be seen that the EXAFS spectrum of Zr1 (about 5 nm) resembles that of YCZ. With increasing particle size, the EXAFS spectrum of nanocrystalline zirconia approaches that of YTZ. This implies that the local environment in nanocrystalline zirconia varies from the local environment in YCZ to that in YTZ.

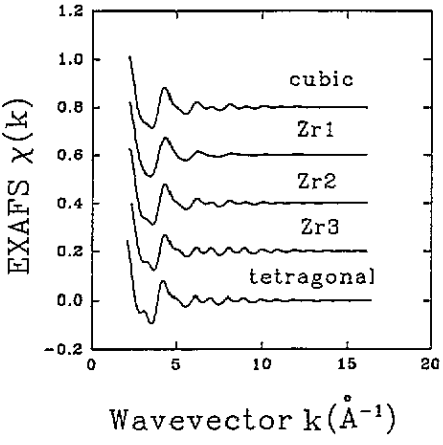

Figure 1. EXAFS $\chi(k)$ spectra of the Zr K edge in nanocrystalline zirconia powders and bulk YCZ and YTZ.

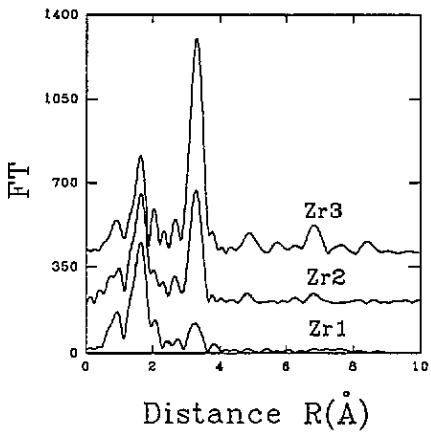

Figure 2. Fourier transforms of the Zr K-edge EXAFS $k^3\chi(k)$ in nanocrystalline zirconia powders.

The Fourier transform (FT) of EXAFS spectra, as shown in figure 2, was carried out within the same scale in k space (from 2.7 $Å^{-1}$ to 14.7 $Å^{-1}$) and with an identical width of Hanning window. The first peaks at about 1.6 Å in FT spectra correspond to the nearest Zr–O shell. It can be seen that the amplitude of this peak for the Zr3 sample is lower than that for the others. The reason for this reduction of amplitude will be given in section 4.2. The second peaks at about 3.2 Å originate from the contribution of Zr–Zr atomic pairs. With a decrease of particle size, the amplitude of the second peak decreases, while the more distant shells disappear rapidly. This implies the breakdown of the long-range order in the structure.

The FT signals for the Zr–O shell and the Zr–Zr shell were isolated respectively with the Fourier filter technique and then backtransformed into k space. A non-linear least-squares

fitting procedure was applied to obtain the local structure parameters. In our case, it is not possible to obtain the backscattering amplitude and phase shift from a reference sample, such as MZ or YCZ, for the complicated coordination environment in these materials [17]. Thus, the theoretically calculated amplitude and phase shift (from FEFF codes [18]) were used in the fitting procedure. The validity of the calculated amplitude and phase shift was verified by using them to fit the experimental spectrum of MZ . The obtained local structural parameters for MZ are consistent with those from single-crystal x-ray diffraction [19]. The fitting parameters for nanocrystalline samples are shown in table 2.

Table 2. Fitting parameters for the Zr–O shell and the Zr–Zr shell (70 K). R, N and σ^2 are the coordination distance, the coordination number and the EXAFS Debye–Waller factor respectively. The first element symbol in the subscript represents the absorbing atom and the second one stands for the backscattering atom.

Sample	R_{Zr-O} (Å)	N_{Zr-O}	σ^2_{Zr-O} ($\times 10^{-3}$ Å^2)	R_{Zr-Zr} (Å)	N_{Zr-Zr}	σ^2_{Zr-Zr} ($\times 10^{-3}$ Å^2)
Zr1	2.120 ± 0.01	6.8 ± 0.7	7.5 ± 1.0	3.587 ± 0.02	4.5 ± 1.0	11.0 ± 1.0
Zr2	2.117 ± 0.01	6.2 ± 0.7	6.7 ± 1.0	3.605 ± 0.01	9.7 ± 0.5	8.0 ± 1.0
Zr3	2.084 ± 0.01	4.5 ± 0.7	3.8 ± 1.0	3.618 ± 0.01	11.1 ± 0.5	5.0 ± 1.0

To extract mean-square relative displacements (MSRDs), the method used by Marcus and co-workers [9] was employed. For each sample, the filtered EXAFS signals at different temperatures were fitted, assuming common values for the coordination distances and coordination numbers and individual values for the MSRDs and energy origin shifts at each temperature. The fitting results are also shown in table 2.

Error bars were estimated in a standard way [20] and are shown in table 2. It should be noted that the error bars of MSRDs were estimated under the same assumption as mentioned above.

4. Discussion

4.1. Interatomic distance

From table 2, we know that the Zr–O bond length contracts with the decrease of particle size, while the Zr–Zr interatomic distance increases. The ratio of Zr–Zr interatomic distance (d_{Zr-Zr}) to Zr–O bond length (d_{Zr-O}) is denoted as R_i. The subscript i represents the label of the sample. The values of R_i for nanocrystalline samples are shown in table 3. Those for the c phase and the t phase [21] are also shown. It should be noted that d_{Zr--Zr} for the t phase takes the average interatomic distance of the two Zr–Zr subshells, and d_{Zr-O} takes the Zr–O distance corresponding to the four nearest oxygen neighbours. With increasing particle size, the R_i value is close to that in the t phase. With decreasing size, the R_i value approaches that in the c phase. This implies the occurrence of a size-induced phase transition. The nanocrystalline zirconia transforms from the t form to the c form with the reduction of crystallite size. Further strong evidence for this kind of phase transition is given in section 4.2. The diffraction study [14, 15] also showed that the lattice parameters approached that of a CaF_2-type structure with decreasing particle size. This result

Table 3. Ratio (R_i) of Zr–Zr interatomic distance to Zr–O bond length.

	Cubic zirconia	Zr1	Zr2	Zr3	Tetragonal zirconia
R_i	1.63	1.69±0.02	1.70±0.01	1.74±0.01	1.78

is consistent with our result, but ours is more determinable, because the EXAFS method does not suffer from the same limitations as the diffraction method.

Our results imply that a size-induced phase transition may occur at some critical crystallite size. However, there is a crystallite size distribution in each sample (the crystallite size determined by XRD is just an average value). The crystallites with different sizes in each sample may be in different phases and hence each sample is a multiphase material. This is the reason why R_i for the nanocrystalline samples changes gradually from the value for the c phase to that for the t phase.

4.2. Coordination number

4.2.1. The coordination number of the Zr–O shell. As shown in table 2, the coordination number of the Zr–O shell decreases with increasing particle size. For samples Zr1 and Zr2, the coordination number approaches seven, close to that for bulk YCZ [17]. However, this value is reduced to 4.5 for sample Zr3. As shown in [17], only four oxygen neighbours are enclosed in the first Zr–O shell for the YTZ sample, and their contribution to the XAFS spectra can be detected. Therefore, the reduction of Zr–O coordination number for Zr3 indicates that Zr3 is in the t phase. This conclusion coincides with that deduced from interatomic distances.

The drop of Zr–O coordination number with increasing of particle size cannot be interpreted as the loss of oxygen atoms on the crystallite surface because if this were so, the decrease of the ratio of surface over volume would make the Zr–O coordination number in Zr3 larger than that in Zr2 or Zr1.

4.2.2. The coordination number of the Zr–Zr shell. For this shell, an obvious feature, as shown in table 2, is the dramatic reduction of coordination number with decreasing particle size. This is due to the particle size effect. Due to the confinement of the crystallite surface, the local environment around central Zr atoms near the surface is different from that around central Zr atoms in the interior. In the former case, the Zr–Zr coordination number decreases, while in the latter case, it keeps the value in the bulk crystal. The Zr–Zr coordination number obtained by EXAFS is the weighted average over both cases. Therefore, with decreasing particle size, the ratio of surface over volume increases and the average Zr–Zr coordination number decreases.

Assuming that the shape of the crystallites is a sphere and the lattice of crystallites is of FCC type, we evaluate the Zr–Zr coordination number. Here, the possible relaxations of surface atoms are neglected. The results calculated, as shown in table 4, are consistent with the experimental ones except for the Zr1 sample. It may be that the morphology of crystallites in the Zr1 sample is very different from a sphere and the lattice relaxation cannot be omitted.

Table 4. Calculated and experimental Zr–Zr coordination numbers. N_0 is the experimental value. N_C is the calculated value.

	Zr1	Zr2	Zr3
N_0	4.5±1.0	9.7±0.5	11.1±0.5
N_C	10.6	11.1	11.4

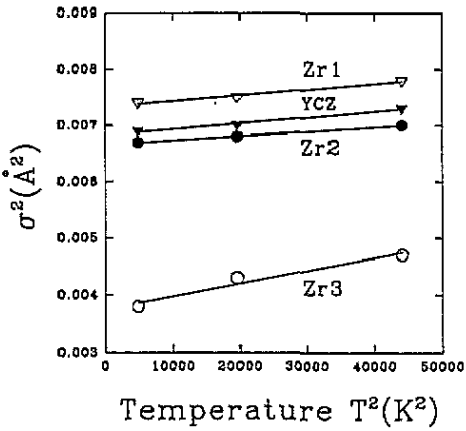

Figure 3. Plot of σ^2 versus T^2 for nanocrystalline zirconia powders and YCZ. Scattered symbols represent experimental data and solid lines are fitting curves. The typical error bar of the experimental data is about ±0.001 (Å^2).

4.3. Thermal vibration

According to the Debye approximation [22], the Debye–Waller factor σ^2 for c zirconia can be expressed as

$$\sigma^2(T) = \sigma_s^2 + \frac{3\hbar^2}{m_r k_B \Theta_D}\left[\frac{1}{4} + \left[\frac{T}{\Theta_D}\right]^2 D_1\right] \tag{1}$$

where σ_s^2 is the statical contribution to the disorder, Θ_D is the Debye temperature and m_r is the reduced mass. D_1 is the slowly varying function

$$D_1\left[\frac{\Theta_D}{T}\right] = \int_0^{\frac{\Theta_D}{T}} \frac{x}{e^x - 1}\,dx.$$

The plots of $\sigma^2(T)$ versus T^2 of the first Zr–O shell for nanocrystalline powders and bulk c zirconia are depicted in figure 3. The best linear fits to these curves according to (1) are also shown. The Debye temperature of bulk yttria-stabilized zirconia is 470 K [23]. Hence, the Debye temperatures of nanocrystalline samples can be obtained from the relative changes of slopes. The values of Debye temperatures thus obtained are shown in table 5. The dramatic drop of Debye temperature for sample Zr3 may be caused by the c–t phase transition. In fact, (1) is not well suited for the Zr3 sample, because the crystal structure of the Zr3 sample deviates from c symmetry. Hence, its Debye temperature is only a qualitative value. However, significant variations are still obvious as shown in figure 3. If we note that the t structure deviates slightly from its c structure, a qualitative comparison between these Debye temperatures is allowable.

Table 5. Debye temperature (Θ_D (K)).

	Zr1	Zr2	Zr3
Θ_D (K)	502	519	404

The variation of σ^2 versus T^2 for nanocrystalline zirconia is about five times lower than that for metal clusters [8]. This reflects the difference between the Zr–O ionic bond (with Θ_D^{bulk} = 160 K) and the Au–Au metal bond (Θ_D^{bulk} = 470 K).

5. Summary and conclusions

In this paper, we have studied the local environment around zirconium ions in a series of nanocrystalline zirconia powders with different particle sizes by the EXAFS method. The analysis of experimental spectra shows that there is a t–c phase transition with reduction of particle size. To our knowledge, there has been no previous report of this transition.

Besides the structural transformation confirmed in this paper, a size-induced t–m phase transition [24] was also observed in the zirconia system. An analogous phase transition has been found in ultrafine Fe_2O_3 [25]. The mechanism of the transformation is complex, because many factors can affect the transition, such as domain boundaries [26], anionic vacancies [27], classical heterogeneous nucleation [28] and the expansion in the unit-cell volume [25]. Further experiments and theoretical consideration would be helpful in understanding the mechanism of this size-induced phase transition.

Acknowledgments

The authors would like to thank Professor Li Chenxi and Mr Li Hefeng for their assistance in experiments. They are also grateful to Xie Yaning, Hu Tiandou and Huang Daxian in the EXAFS station at Beijing Synchrotron Radiation Laboratory for their technical support during the EXAFS measurements. This work is supported by the Chinese National Science Foundation.

References

[1] Karch J, Birringer R and Gleiter H 1987 *Nature* **330** 556–8
[2] Schumacher S, Birringer R, Strauss R and Gleiter H 1989 *Acta Metall.* **37** 2485–8
[3] Fitzsimmons M R, Eastman J A, Müller-Stach M and Wallner G 1991 *Phys. Rev.* B **44** 2452–60
[4] Wunderlich W, Ishida Y and Maurer R 1990 *Scr. Metall.* **24** 403–8
[5] Thomas G T, Siegel R W and Eastman J A 1990 *Scr. Metall.* **24** 201–6
[6] Schaefer H E, Wuerschum R, Birringer R and Gleiter H 1988 *Phys. Rev.* B **28** 9545–54
[7] Ramasamy S, Jiang R, Gleiter H, Birringer R and Gonser U 1990 *Solid State Commun.* **74** 851–5
[8] Balerna A, Bernieri P, Reale A, Santucci S, Burattini E and Mobilio S 1985 *Phys. Rev.* B **31** 5058–65
[9] Marcus M A, Andrews M P, Zegenhagen J, Bommannavar A S and Montano P 1990 *Phys. Rev.* B **42** 3312–6
[10] Yokoyama T and Ohta T 1990 *Japan. J. Appl. Phys.* **29** 2052–8
[11] Montano P A, Shenoy G K and Alp E E 1986 *Phys. Rev. Lett.* **56** 2076–9
[12] Mitsuhashi T, Ichihara M and Taksuke U 1974 *Phys. Rev. Lett.* **57** 97
[13] Chen I W and Chiao Y H 1983 *Acta. Metall.* **31** 1627
[14] Srinivasan R, De Angelis R J, Ice G and Davis B H 1991 *J. Mater. Res.* **6** 1287–92

[15] Petrunin V F, Ermolaev A G, Burkhanov A V, Knyazev E V, Trusov L I, Zelikman A N and Vasil'ev S A 1989 *Sov. Powder Metall. Met. Ceram.* **28** 199–203
[16] Sayers D E and Bunker B A 1988 *X-ray Absorption: Principles, Applications and Techniques of EXAFS, SEXAFS and XANES* ed D C Koningsberger and R Prins (New York: Wiley) ch 6
[17] Tuilier M H, Dexpert-Ghys J, Dexpert H and Lagarde P 1987 *J. Solid State Chem.* **69** 153–61
[18] Rehr J J, Mustre de Leon J, Zabinsky S I, and Albers R C 1991 *J. Am. Chem. Soc.* **113** 5135
[19] Smith D K and Newkirk H W 1965 *Acta Crystallogr.* **18** 983
[20] Lytle F W, Sayers D E and Stern E A 1989 *Physica* B **158** 701
[21] Teufer G 1962 *Acta Crystallogr.* **15** 1187
[22] Beni G and Platzman P M 1976 *Phys. Rev.* B **14** 1514
[23] Lawless W N *Phys. Rev.* B **21** 585–8
[24] Garvie R C and Goss M F 1986 *J. Mater. Sci.* **21** 1253–7
[25] Ayyub P, Multani M, Barma M, Palkar V R and Vijayaraghavan R 1988 *J. Phys. C: Solid State Phys.* **21** 2229–45
[26] Mitsuhashi T, Ichihara M and Tatsuke U 1974 *J. Am. Ceram. Soc.* **57** 97–101
[27] Osendi M I, Moya J S, Serna C J and Soria J 1985 *J. Am. Ceram. Soc.* **68** 135–9
[28] Chen I W and Chiao Y H 1983 *Acta Metall.* **31** 1627–38